Simultaneous multiplicity and forward energy characterization of particle spectra in Au+Au collisions at 11.6*A* GeV/*c*

L. Ahle,[9,*] Y. Akiba,[6] K. Ashktorab,[1] M. D. Baker,[9,†] D. Beavis,[1] H. C. Britt,[7] J. Chang,[3] C. Chasman,[1] Z. Chen,[1,‡] C.-Y. Chi,[4] Y. Y. Chu,[1] V. Cianciolo,[9,§] B. A. Cole,[4] H. J. Crawford,[2] J. B. Cumming,[1] R. Debbe,[1] J. C. Dunlop,[9] W. Eldredge,[3] J. Engelage,[2] S.-Y. Fung,[3] E. Garcia,[8] S. Gushue,[1] H. Hamagaki,[10] L. F. Hansen,[7] R. S. Hayano,[11] G. Heintzelman,[9] E. Judd,[2] J. Kang,[13] E.-J. Kim,[1,13] A. Kumagai,[12] K. Kurita,[12,‖] J.-H. Lee,[1] J. Luke,[7] Y. Miake,[12] A. Mignerey,[8] B. Moskowitz,[1] M. Moulson,[4] C. Muentz,[1,¶] S. Nagamiya,[5] M. N. Namboodiri,[7] C. A. Ogilvie,[9] J. Olness,[1] L. P. Remsberg,[1] H. Sako,[11,**] T. C. Sangster,[7] R. Seto,[3] J. Shea,[8] K. Shigaki,[11,††] R. Soltz,[9,*] S. G. Steadman,[9] G. S. F. Stephans,[9] M. J. Tannenbaum,[1] J. H. Thomas,[7,‡‡] S. Ueno-Hayashi,[12] F. Videbaek,[1] F. Wang,[4,‡‡] Y. Wu,[4] H. Xiang,[3] G. H. Xu,[3] K. Yagi,[12] H. Yao,[9] W. A. Zajc,[4] and F. Zhu[1]

(E-802 Collaboration)

[1]*Brookhaven National Laboratory, Upton, New York 11973*
[2]*University of California, Space Sciences Laboratory, Berkeley, California 94720*
[3]*University of California, Riverside, California 92507*
[4]*Columbia University, New York, New York 10027 and Nevis Laboratories, Irvington, New York 10533*
[5]*High Energy Accelerator Research Organization (KEK),Tsukuba, Ibaraki 305, Japan*
[6]*High Energy Accelerator Research Organization (KEK), Tanashi-branch, (Tanashi) Tokyo 188, Japan*
[7]*Lawrence Livermore National Laboratory, Livermore, California 94550*
[8]*University of Maryland,College Park, Maryland 20742*
[9]*Massachusetts Institute of Technology, Cambridge, Massachusetts 02139*
[10]*Center for Nuclear Study, School of Science, University of Tokyo, Tanashi, Tokyo 188, Japan*
[11]*Department of Physics, University of Tokyo, Tokyo 113, Japan*
[12]*University of Tsukuba, Tsukuba, Ibaraki 305, Japan*
[13]*Yonsei University, Seoul 120-749, Korea*

(Received 28 October 1998)

In this paper Au+Au collisions at 11.6*A* GeV/*c* are characterized by two global observables: the energy measured near zero degrees (E_{ZCAL}) and the total event multiplicity. Particle spectra are measured for different event classes that are defined in a two-dimensional grid of both global observables. For moderately central events ($\sigma/\sigma_{\mathrm{int}}<12\%$) the proton dN/dy distributions do not depend on E_{ZCAL} but only on the event multiplicity. In contrast the shape of the proton transverse spectra shows little dependence on the event multiplicity. The change in the proton dN/dy distributions suggests that different conditions are formed in the collision for different event classes. These event classes are studied for signals of new physics by measuring pion and kaon spectra and yields. In the event classes doubly selected on E_{ZCAL} and multiplicity there is no indication of any unusual pion or kaon yields, spectra, or K/π ratio even in the events with extreme multiplicity. [S0556-2813(99)03704-8]

PACS number(s): 25.75.−q, 13.85.Ni

I. INTRODUCTION

Collisions between two heavy nuclei at beam energies of 11*A* GeV/*c* form extended regions of dense nuclear matter. Because of the stochastic nature of the collisions, each reaction produces a different system, even for the same initial impact parameter. In particular the baryon and energy density can vary from event to event. If it is possible to experimentally select events that have the largest volume of dense matter, then these events can be probed for signals of new physics, e.g., the formation of a baryon-rich quark-gluon plasma (QGP).

*Present address: Lawrence Livermore National Laboratory, Livermore, CA 94550.
†Present address: Brookhaven National Laboratory, Upton, NY 11973.
‡Present address: Renaissance Technologies Corp., Stony Brook, NY 11790.
§Present address: Oak Ridge National Laboratory, Oak Ridge, TN 37831.
‖Present address: The Institute of Physical and Chemical Research (RIKEN), Saitama 351-01, Japan.
¶Present address: Goethe Universitaet, Institut fuer Kernphysik, Frankfurt, Germany.
**Present address: University of Tsukuba, Tsukuba, Ibaraki 305, Japan.
††Present address: High Energy Accel Res. Organization (KEK), Tsukuba, Ibaraki 305, Japan
‡‡Present address: Lawrence Berkeley National Laboratory, Berkeley, CA 94720.

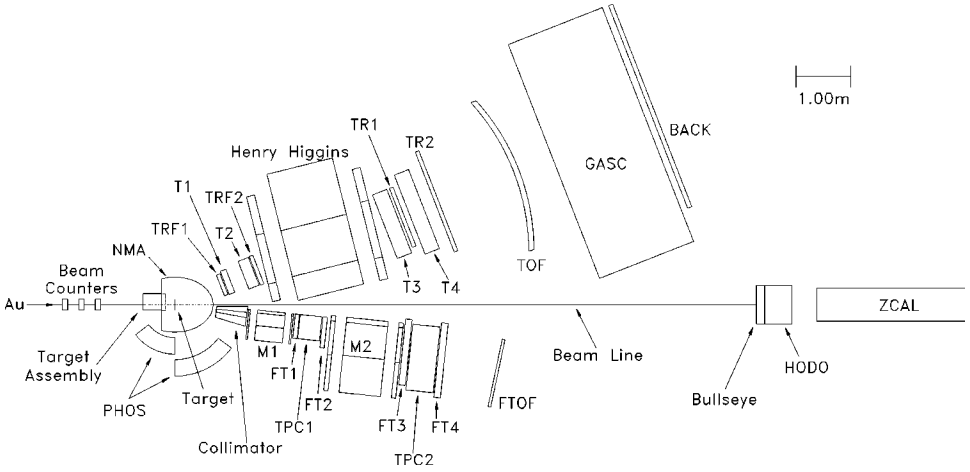

FIG. 1. The experimental layout of E866 in the Fall of 1994 showing the multiplicity array (NMA), the zero-degree calorimeter (ZCAL), the interaction trigger (Bullseye), and the Henry Higgins spectrometer consisting of drift chambers (T1-T4), wire chambers (TRF1,2 and TR1,2), a time-of-flight wall (TOF) and a gas-Cerenkov detector (GASC). The forward spectrometer consists of a sweeping magnet (M1), analyzing magnet (M2), drift chambers (FT1-4), two time projection chambers (TPC1,2) and a time-of-flight wall (FTOF). A scintillator array (PHOS) for particle spectra at back angles and a hodoscope (HODO) of crossed XY slats complete the detector hardware of E866.

In the spectator-participant model [1] of heavy-ion reactions, a projectile spectator nucleon is one that did not collide with a target nucleon. The number of spectator nucleons is determined by the initial stage of the reaction and at relativistic beam energies, these spectator nucleons dominate the energy measured near the polar angle of zero degrees. In contrast, the multiplicity of the event depends on the full history of the reaction: from the initial energy deposited by beam and target nucleons, to the secondary hadron-hadron collisions.

This paper reports on data taken in the fall of 1994 by experiment E866 at the AGS using a Au target and the 11.6*A* GeV/*c* Au beam. It presents the correlation between these two global observables, the energy near zero degrees and the event multiplicity. As such, it is a continuation of our study of Si+*A* reactions at 14.6*A* GeV/*c* [2] that examined the correlation between two similar global measures of an event, zero-degree energy and transverse energy. In Au reactions, the distribution of a single global observable, transverse energy, has been reported by experiment E877 [3]. In addition, several authors [4–6] have predicted that high multiplicity events could indicate the onset of the quark-gluon plasma. The extra entropy in the quark phase could manifest itself as a large number of produced hadrons in the final state. Kapusta *et al.* [6] have speculated that rare high multiplicity events could come from rapidly growing droplets of plasma, and reported here is a search for such high multiplicity events.

Most importantly, this paper presents particle spectra from different event classes that have been simultaneously selected on two global variables, the energy near zero degrees and the event multiplicity. To do this quantitatively, it defines event classes in a grid of two-dimensional cuts in the zero-degree energy and the event multiplicity. For each event class, the yield and spectra of particles emitted in these reactions are measured with a spectrometer. To our knowledge this is the first time an event selection based on more than one global observable has been used to study the spectra of particles emitted in high-energy nuclear reactions. Proton spectra in these event classes are used to study whether the reactions produce different conditions in the participating matter. These events are then probed for signals of new physics using the spectra and yields of produced particles, pions and kaons. This paper therefore extends our previous results on proton and pion spectra in Au+Au central collisions [7] by studying how these spectra evolve as a function of global observables.

Section II describes experiment E866 at the AGS and the methods used to analyze the data. Section III defines the event selection in a two-dimensional grid of zero-degree energy and event multiplicity as well as event selection solely on zero-degree energy, while Sec. IV contains the measured proton distributions for each event class. The spectra and yields of the produced particles K^+ and π^+ for each event class are described in Secs. V and VI. The conclusions are presented in Sec. VII.

II. EXPERIMENT AND DATA ANALYSIS

The E866 apparatus [7,8] consists of event-characterizing global detectors and two magnetic spectrometers as is shown in Fig. 1. Details of the experiment and data analysis can be found in Refs. [7,9].

This paper uses data from the Henry Higgins spectrometer. In the 1994 running period one of the global detectors used in this paper (the New Multiplicity Array) was installed after the Forward spectrometer had completed its data collection. The Henry Higgins spectrometer has a 25 msr solid angle, with $\Delta\theta \sim 14°$. By rotating the spectrometer, the acceptance covers lab angles from $14-58°$. The spectrometer has a combination of drift and multiwire chambers to locate the tracks before and after a dipole magnet.

Experiment 866 has two detectors that measured the global characteristics of each event, a multiplicity array (NMA) and a Fe-scintillator sandwich type calorimeter (ZCAL) with an 1.5° opening angle around the beam-axis. The calorimeter is 138 layers of 0.4 cm thick scintillator alternating with 138 layers of 1.0 cm thick iron. Each sheet is 60 cm by 60 cm and is centered on the beamline. The front face of the calorimeter is 11.7 m from the target. For more details on the

readout of this device the reader is referred to Beavis *et al.* [10]. The energy deposited into this calorimeter is designated E_{ZCAL}. The calorimeter was calibrated to maintain the fragmented-beam peak at the kinetic energy of the beam, $E_{\mathrm{beam}}^{\mathrm{kin}}=2123$ GeV. Fragmented-beam events are those that react just upstream of the calorimeter. This calibration was performed for each run to compensate for the radiation-damage decrease in calorimeter light output. The decrease in light-output over the entire 1994 running period was 7%. The resolution of E_{ZCAL} is discussed in Sec. III.

The second global detector was the New Multiplicity Array (NMA). This detector was added to E866 in 1994 and because this is the first paper to use the NMA, the detector is described in detail here. The major design goal for this array was to measure the multiplicity of produced particles while excluding the protons that mainly come from the original beam and target nuclei. Hence each module in the array was made out of 5 cm thick ultra-violet-transmitting lucite which acts as a Cerenkov radiator for particles with $\beta>0.6$. From Monte Carlo simulations of a NMA module the effective β-threshold for particles to produce sufficient light to be counted as a hit is $\beta>0.8$. This filtered out the slow protons whereas most of the pions were above the Cerenkov threshold.

A thin sheet of lead was put in front of the lucite to convert γ's to e^+e^- pairs. Both the e^+ and e^- will radiate Cerenkov light and hence a single γ that has converted will be detected as two charged particles. The major source of γ's in Au-Au collisions is π^0 decay. The thickness of the lead, 1.7 mm, was chosen so that the probability of converting a γ is 1/4, and the NMA will on average record a multiplicity of one for every π^0.

Three hundred and forty-six modules in the NMA covered an angular range $-0.4<\eta<2.8$. The device has 14 separate rings, where each ring covers a slice in η. Within each η slice, a single NMA module covers a small range of azimuthal angle. The shape of each module was therefore a truncated pyramid with curved sides. The NMA acceptance and segmentation are listed in Table I, together with the details of the azimuthal gaps left for the spectrometers' acceptance. For example, from Table I, the 6th ring has a 40° gap between $-20°<\phi<20°$ on the forward spectrometer side of the experiment and a 60° gap between $-180°<\phi<-150°$ and $150°<\phi<180°$ on the Henry Higgins side. Each NMA module was optically glued to a photomultiplier tube. The forward five rings used Hamamatsu H3165-01 tubes while the remaining back rings used Hamamatsu H268 tubes.

Multiple particles hitting a module are analyzed using the analog signal from the photomultiplier tube. One and two particle peaks are observed (Fig. 2). The calibrated amplitude (h_i) of each NMA module is transformed to the average module multiplicity [$W(h_i)$] that would generate this signal,

$$W(h_i)=\frac{\sum_{n=1} nA_nS(h_i,n)}{\sum_{n=1} A_nS(h_i,n)}, \quad h_i>0.5, \tag{1}$$

where $S(h_i,n)$ is the Gaussian response function for a module that is hit by n particles

TABLE I. Table of η and ϕ coverage of the NMA, r is the distance from the target to the front of each module, $\Delta\phi$ is the ϕ acceptance of each module in a ring of a fixed η slice, and modules is the number of modules in that ring. ϕ_{min} and ϕ_{max} refer to range of azimuthal angles in the top half of the NMA. The top and bottom half of the array are symmetric across the xz plane.

Ring	η_{max}	η_{min}	r (c.m.)	$\Delta\phi$	Modules	ϕ_{min}	ϕ_{max}
1	2.8	2.4	50.8	20°	6	70°	130°
2	2.4	2.1	50.8	15°	12	52.5°	142.5°
3	2.1	1.85	50.8	12°	20	36°	156°
4	1.85	1.6	50.8	10°	26	30°	160°
5	1.6	1.4	49.8	10°	26	30°	160°
6	1.4	1.2	48.8	10°	26	20°	150°
7	1.2	1.0	46.8	10°	26	20°	150°
8	1.0	0.8	44.8	10°	28	10°	150°
9	0.8	0.6	42.8	10°	28	10°	150°
10	0.6	0.4	39.8	10°	28	10°	150°
11	0.4	0.2	36.8	10°	30	0°	150°
12	0.2	0.0	34.8	10°	30	0°	150°
13	0.0	-0.2	34.8	10°	30	0°	150°
14	-0.2	-0.4	34.8	10°	30	0°	150°

$$S(h_i,n)=\frac{1}{\sigma_n\sqrt{2\pi}}e^{-(h_i-n)^2/(2\sigma_n^2)}. \tag{2}$$

The relative probability, A_n, for a given module to be hit by n particles is estimated using two Poisson distributions [$P(j:\mu)$], one for charged particles and one for photons that convert in the Pb layer and contribute two hits to the module.

$$A_n=\sum_{i=0}^{n/2} P(2i:\mu_{\mathrm{charged}})\times P(n/2-i:\mu_{\mathrm{photon}}), \quad n=\text{even},$$

$$A_n=\sum_{i=0}^{(n-1)/2} P(2i+1:\mu_{\mathrm{charged}})\times P((n-1)/2-i:\mu_{\mathrm{photon}}), \quad n=\text{odd}. \tag{3}$$

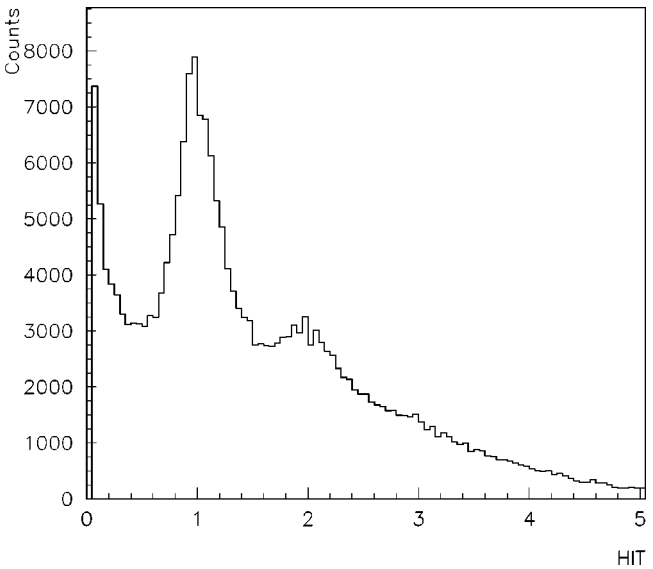

FIG. 2. The calibrated hit distribution summed over all the NMA modules in ring 5 (Table I).

The mean values ($\mu_{\text{charged}}, \mu_{\text{photon}}$) of the Poisson distributions were determined from fits to semi-inclusive NMA module spectra (Fig. 2). The increase of the mean values with centrality was parametrized for each η ring as a function of the raw multiplicity Σh_i of the event. The widths (σ_n) for the Gaussian response functions [Eq. (2)] increase with n as $\sigma_n = \sqrt{n} \times \sigma_1$, where σ_1 is the fitted width of the first peak of the NMA module spectra. The multiplicity of an event, mult_{NMA}, is the sum of $W(h_i)$ [Eq. (1)] over all the modules in the NMA.

The single-track reconstruction efficiency for the Henry Higgins spectrometer was determined by simulating a single track through the E866 GEANT [11] Monte Carlo and track reconstruction program. This provides the efficiency of the tracking algorithm for fully efficient hardware as a function of the momentum of the particle. As an example, the tracking efficiency for protons is found to have the functional form $\epsilon_{\text{proton}} = A_0(1 - A_1/\beta^2 p^2)$ where $A_0 = 0.975$ and $A_1 = 0.0086$. For protons in the spectrometer, with typical values of momenta, this tracking efficiency ranges from 90% to 95%. The hardware efficiencies of the tracking chambers of the Henry Higgins spectrometer were found to be very close to 100%.

Tracks are also lost because of hit blocking caused by the finite occupancy of chambers and TOF walls. This loss of tracks was estimated by embedding hits from isolated, single tracks from peripheral collisions into other events. The combined event was reanalyzed to determine if the embedded track was still reconstructed by the tracking program. The resulting blocking-induced inefficiency was parametrized as a function of the overall occupancy of the Henry Higgins spectrometer and as a function of position both in front and behind the dipole magnet. For the most central event class and tracks at forward angles, the blocking-inefficiency was $40 \pm 10\%$. This inefficiency reduces to $10 \pm 5\%$ at back angles. From the embedding studies, approximately half of the blocking inefficiency was caused by multiple hits on a slat in the TOF wall.

The systematic uncertainty on the normalization of the measured invariant spectra and rapidity distributions is dominated by uncertainty in the tracking efficiency and loss of tracks due to hit-blocking. The tracking uncertainty increases from 5 to 10% the closer to midrapidity and the more central the event class. For peripheral collisions, there is a 10% uncertainty in the cross section of the event class. This reduces to 5% for central collisions. There are small contributions to the uncertainty from the acceptance of the spectrometer and particle identification losses. This leads to a total systematic uncertainty in the normalization of 15% independent of centrality.

The systematic uncertainty on the mean transverse momentum is estimated to be 5% and is dominated by uncertainty in the tracking efficiency and acceptance.

III. EVENT CLASSIFICATION

Figure 3 shows the E_{ZCAL} distribution for interaction events before and after target-out subtraction. The energy deposited into the calorimeter is dominated by projectile spectator nucleons. The number of projectile participants (N_{pp}) is estimated by inverting the measured E_{ZCAL}

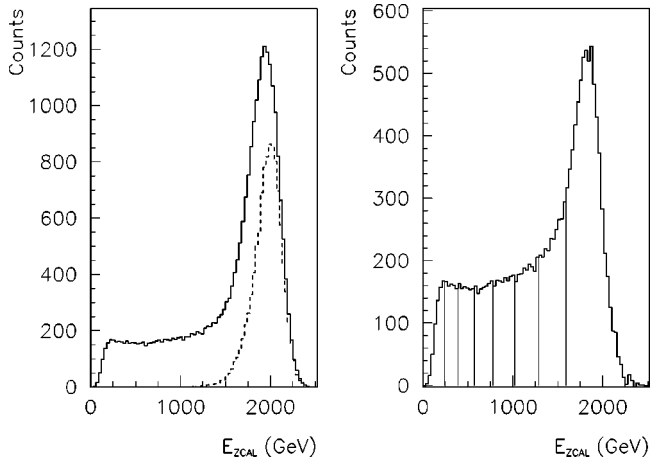

FIG. 3. Left panel: the distribution of E_{ZCAL} for interaction events in Au+Au reactions at 11.6A GeV/c for target-in and target-out (dashed line) runs. The right panel is after target-out subtraction. The lines indicate the event selection cuts in Table II.

$$N_{pp} = 197 \times \left(1 - \frac{E_{\text{ZCAL}}}{E_{\text{beam}}^{\text{kin}}}\right), \tag{4}$$

where $E_{\text{beam}}^{\text{kin}} = 2123$ GeV is the kinetic energy of the beam.

For peripheral collisions, the calorimeter has a slight nonlinear response, with a 4% reduction in output for beam events that did not react compared to events that fragment just upstream of the calorimeter. This leads to an uncertainty of up to eight in the value of N_{pp}, or 30%, only for the most peripheral event class (Table II).

Mesons entering the acceptance of the calorimeter also contribute to the measured E_{ZCAL} [2]. By passing events from a cascade model [12] through a simulation of the calorimeter, the meson energy contribution is estimated to be the equivalent of three projectile nucleons for the most central event class (Table II). It is proportionally smaller for less central bins. The mesonic contribution was not subtracted from E_{ZCAL}.

TABLE II. Table listing the borders of E_{ZCAL} when E_{ZCAL} is solely used for event selection. Also listed is the corresponding range of the inelastic cross section, in mb, and the percentage in reference to the total inelastic cross section of 6.8 b. The last column is the average value of N_{pp} for interaction events in that event class.

E_{ZCAL} class	E_{ZCAL} range (GeV)	Cross section (mb)	% σ_{int}	$\langle N_{\text{pp}} \rangle$
1	0–240	0–212	0–3	181
2	240–390	212–484	3–7	168
3	390–570	484–799	7–12	152
4	570–780	799–1174	12–17	134
5	780–1020	1174–1613	17–24	113
6	1020–1290	1613–2183	24–32	89.5
7	1290–1590	2183–2976	32–43	62.5
8	>1590	2976–5130	43–76	26.9

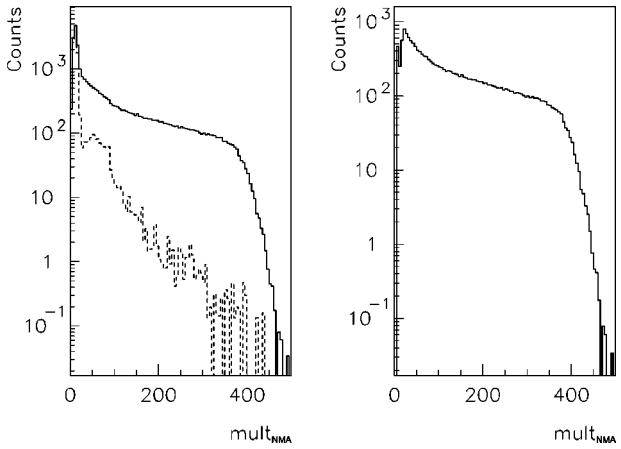

FIG. 4. Left panel: the distribution of mult_{NMA} for interaction events in Au+Au reactions at 11.6*A* GeV/*c* for target-in and target-out (dashed line) runs. The right panel is after target-out subtraction.

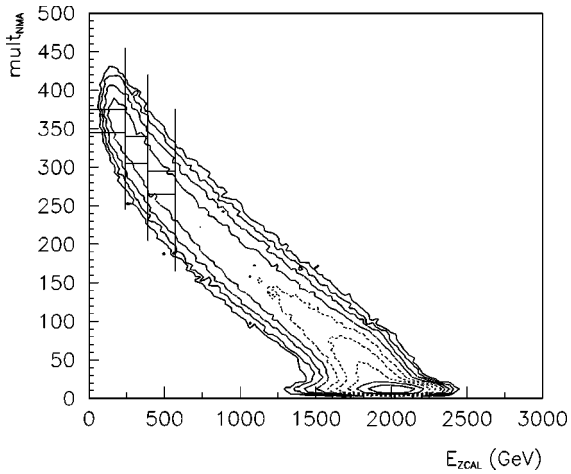

FIG. 5. The correlation in Au+Au reactions at 11.6*A* GeV/*c* between the two global measures of an event, mult_{NMA} and E_{ZCAL}, for interaction events after target-out subtraction. The lines indicate the two-dimensional grid used to select events and the contours are plotted on a logarithmic scale.

N_{pp} should therefore be considered an experimental observable [defined by the measured E_{ZCAL}, Eq. (4)] and provides an estimate of the geometrical number of projectile participants.

Table II lists the cuts used when E_{ZCAL} is solely used for event selection. From the width of the fragmented beam peak, the resolution of the calorimeter is estimated to be

$$\sigma_E = a\sqrt{E_{\text{ZCAL}}}, \quad a = 2.9 \ \text{GeV}^{1/2}. \tag{5}$$

The NMA measured multiplicity, mult_{NMA}, also distinguishes between peripheral and central events. Figure 4 shows the mult_{NMA} distribution for interaction events before and after target-out subtraction. For high multiplicity events, there is a smooth fall-off of yield. There is no indication of the predicted shoulder or extra group of rare high multiplicity events [6].

The detector resolution for the NMA is

$$\sigma_{\text{det}} = \sigma_1\sqrt{\text{mult}_{\text{NMA}}}, \tag{6}$$

where mult_{NMA} is the total measured multiplicity and $\sigma_1 = 0.3$ is the measured resolution of a single module with one incident particle.

The two global observables, mult_{NMA} and E_{ZCAL}, are correlated (Fig. 5). The average multiplicity increases nonlinearly with decreasing values of E_{ZCAL}, similar to the observation in Si+*A* reactions [2]. The width of this correlation is a combination of the resolution of both global detectors and any physics fluctuation in the event multiplicity and forward energy. Various studies were performed examining the distribution of measured mulltiplicities at a fixed value of E_{ZCAL}, and the distribution of E_{ZCAL} at a fixed multiplicity. These distributions were broader than the estimated resolution of the detectors. However, a good indication that the width in the correlation is significant is seen from particle spectra as measured in the spectrometer as a function of event-classes selected simultaneously on both E_{ZCAL} and multiplicity as discussed below.

In the following sections, events will be classified by a grid of two-dimensional cuts in E_{ZCAL} and mult_{NMA}. This grid is indicated on Fig. 5 and Table III lists the values used

TABLE III. Table listing the borders for the double-event selection using E_{ZCAL} and mult_{NMA}. Also listed are the labels used for the event classes, an index for each E_{ZCAL} and mult_{NMA} range. The average value of mult_{NMA} for interaction events in each doubly-selected event class is also provided. The cross section for E_{ZCAL} class 1 is 0–3 % of $\sigma_{\text{int}} = 6.8$ b (summed over all mult_{NMA}), for E_{ZCAL} class 2 is 3–7 %, and for E_{ZCAL} class 3 is 7–12 %.

E_{ZCAL} range	mult_{NMA} range	E_{ZCAL} class	mult_{NMA} class	Average mult_{NMA}
0–240	>375	1	1	394.7
0–240	345–375	1	2	360.5
0–240	<345	1	3	323.2
240–390	>340	2	1	363.5
240–390	305–340	2	2	322.5
240–390	<305	2	3	281.0
390–570	>295	3	1	319.0
390–570	265–295	3	2	280.1
390–570	<265	3	3	240.7

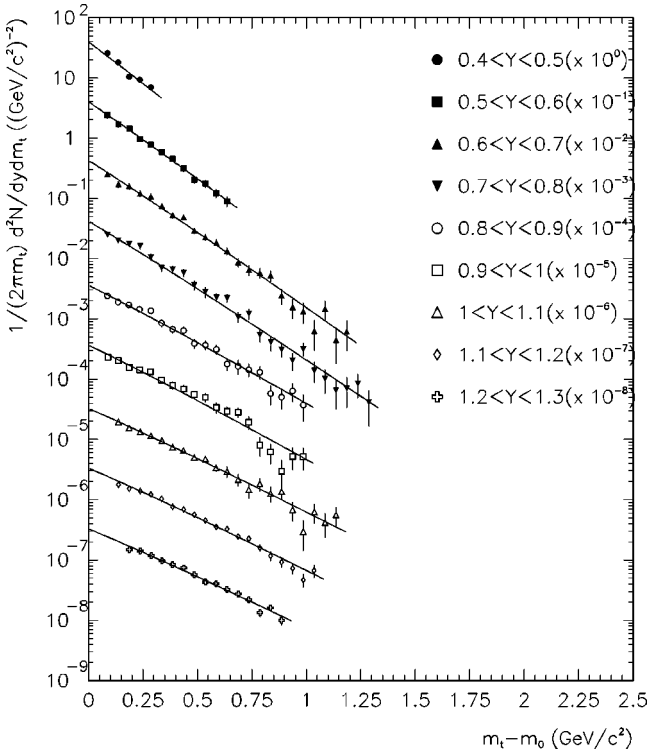

FIG. 6. The proton invariant spectra as a function of m_T for the geometrically most central Au+Au events at 11.6*A* GeV/c with the highest multiplicity (E_{ZCAL} class 1 $\mathrm{mult}_{\mathrm{NMA}}$ class 1 in Table III). The spectra for each rapidity slice are divided by successive powers of ten for clarity. The lines are fits to the data with the Boltzmann functional form [Eq. (7)].

in the double event selection. Within each E_{ZCAL} cut, the $\mathrm{mult}_{\mathrm{NMA}}$ cuts were chosen to obtain approximately equal and statistically significant number of events in each event class.

IV. PROTON SPECTRA

For each event class the shape of the proton rapidity distribution probes how much energy is transferred from the initial beam direction and made available for particle production and transverse expansion.

In Fig. 6 typical invariant cross sections, divided by the reaction cross section for the event class, are plotted for protons as a function of transverse mass and rapidity. Transverse mass is $m_t=\sqrt{p_t^2+m_0^2}$ where p_t is the transverse momentum and m_0 is the rest mass of the particle. These spectra are the invariant differential yield of protons per event. The event class has been doubly selected on the lowest values of E_{ZCAL} and the highest multiplicities (E_{ZCAL} class 1 $\mathrm{mult}_{\mathrm{NMA}}$ class 1 in Table III).

These proton spectra can be fit with a variety of functional forms, including a double exponential [7] or a Boltzmann function; the choice of either a Boltzmann or double exponential fitting function changes the values of these extracted spectral characteristics by less than 5%. The fit to proton spectra is primarily used to extract the rapidity density, dN/dy, and mean m_t,$\langle m_t\rangle$, in each rapidity slice.

Throughout this paper the proton spectra are fitted with a function of Boltzmann form

$$\frac{1}{2\pi m_t}\frac{d^2N}{dm_t dy}=\frac{dN/dy}{2\pi(m_0^2T_B+2m_0T_B^2+2T_B^3)}m_t \times e^{-(m_t-m_0)/T_B}. \tag{7}$$

The two fit parameters are the rapidity density, dN/dy, and the inverse slope parameter, T_B. From the inverse slope parameter the mean m_t,$\langle m_t\rangle$, is calculated

$$\langle m_t\rangle=\frac{m_0^3+3m_0^2T_B+6m_0T_B^2+6T_B^3}{m_0^2+2m_0T_B+2T_B^2}. \tag{8}$$

In Fig. 7 the proton dN/dy is plotted for each event class that was doubly selected on E_{ZCAL} and $\mathrm{mult}_{\mathrm{NMA}}$ (Table III). The dN/dy distributions are tabulated in Table IV. The panels in this plot are arranged in the same graphical position as the two-dimensional grid of $\mathrm{mult}_{\mathrm{NMA}}$ and E_{ZCAL} cuts in Fig. 5. Each column corresponds to a range in E_{ZCAL}, with the most central reactions on the left. Within a range of E_{ZCAL}, the multiplicity of the events increases from bottom to top.

In each E_{ZCAL} range the low multiplicity events have a broad proton dN/dy distribution. Increasing the event multiplicity narrows the width of the proton dN/dy. This change of width is quantified in Fig. 8, where the restricted root-mean-squared (rms) value is denoted dN/dy_{rms}

$$dN/dy_{\mathrm{rms}}=\sqrt{\frac{\sum dN/dy(y-y_{nn})^2}{\sum dN/dy}} \tag{9}$$

of each proton dN/dy distribution is plotted. The rms is calculated in the restricted range $0.35<y<1.35$ with y_{nn}

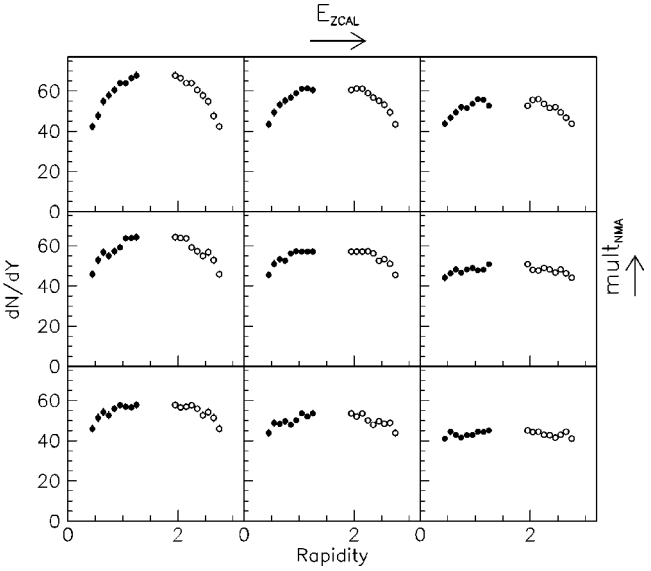

FIG. 7. The proton dN/dy distributions from Au+Au reactions at 11.6*A* GeV/c are plotted for each event class doubly selected on $\mathrm{mult}_{\mathrm{NMA}}$ and E_{ZCAL} (Table III). Each column corresponds to a range in E_{ZCAL} with the most geometrically central events in the left column. For a given E_{ZCAL}, the multiplicity increases from bottom to top. The open points are the data reflected about midrapidity.

TABLE IV. The dN/dy and $\langle m_t \rangle - m_0$ distributions for protons in Au+Au reactions at 11.6A GeV/c for each event class doubly selected on E_{ZCAL} and $\mathrm{mult}_{\mathrm{NMA}}$ (Table III).

y	dN/dy	$\langle m_t \rangle - m_0$ (GeV)	y	dN/dy	$\langle m_t \rangle - m_0$ (GeV)	y	dN/dy	$\langle m_t \rangle - m_0$ (GeV)
				E_{ZCAL} class 1, $\mathrm{mult}_{\mathrm{NMA}}$ class 1				
0.45	42.3±1.7	0.176±0.022	0.55	47.7±1.9	0.194±0.007	0.65	54.9±1.9	0.208±0.004
0.75	57.9±1.9	0.222±0.005	0.85	60.6±1.7	0.264±0.009	0.95	64.0±1.6	0.274±0.008
1.05	63.9±1.5	0.304±0.010	1.15	66.5±1.6	0.308±0.008	1.25	67.8±1.8	0.319±0.010
				E_{ZCAL} class 1, $\mathrm{mult}_{\mathrm{NMA}}$ class 2				
0.45	45.8±1.7	0.198±0.023	0.55	52.9±1.9	0.202±0.007	0.65	56.7±1.9	0.218±0.004
0.75	54.9±1.7	0.233±0.005	0.85	57.3±1.6	0.246±0.007	0.95	59.2±1.4	0.268±0.008
1.05	63.8±1.5	0.290±0.009	1.15	63.9±1.5	0.305±0.008	1.25	64.3±1.8	0.312±0.010
				E_{ZCAL} class 1, $\mathrm{mult}_{\mathrm{NMA}}$ class 3				
0.45	46.0±1.8	0.208±0.027	0.55	51.4±2.0	0.199±0.008	0.65	54.2±1.9	0.217±0.005
0.75	52.7±1.8	0.233±0.005	0.85	55.9±1.6	0.256±0.010	0.95	57.6±1.5	0.273±0.009
1.05	56.9±1.5	0.278±0.009	1.15	56.6±1.5	0.295±0.008	1.25	57.9±1.7	0.316±0.011
				E_{ZCAL} class 2, $\mathrm{mult}_{\mathrm{NMA}}$ class 1				
0.45	43.4±1.7	0.167±0.017	0.55	49.4±1.8	0.198±0.007	0.65	53.1±1.7	0.214±0.004
0.75	55.2±1.7	0.231±0.004	0.85	56.8±1.5	0.251±0.007	0.95	58.9±1.4	0.270±0.007
1.05	61.2±1.4	0.270±0.007	1.15	61.4±1.4	0.308±0.008	1.25	60.4±1.6	0.316±0.010
				E_{ZCAL} class 2, $\mathrm{mult}_{\mathrm{NMA}}$ class 2				
0.45	45.5±1.5	0.181±0.017	0.55	51.1±1.7	0.199±0.006	0.65	53.4±1.6	0.216±0.004
0.75	52.5±1.5	0.231±0.004	0.85	56.2±1.4	0.253±0.006	0.95	57.3±1.3	0.261±0.007
1.05	57.2±1.3	0.273±0.008	1.15	57.2±1.3	0.282±0.006	1.25	57.2±1.4	0.309±0.009
				E_{ZCAL} class 2, $\mathrm{mult}_{\mathrm{NMA}}$ class 3				
0.45	43.8±1.8	0.227±0.027	0.55	48.8±1.6	0.214±0.007	0.65	48.4±1.5	0.223±0.004
0.75	49.7±1.5	0.239±0.005	0.85	48.0±1.3	0.253±0.008	0.95	50.2±1.2	0.262±0.007
1.05	53.6±1.3	0.256±0.008	1.15	52.1±1.3	0.290±0.008	1.25	53.6±1.5	0.305±0.010
				E_{ZCAL} class 3, $\mathrm{mult}_{\mathrm{NMA}}$ class 1				
0.45	43.8±1.5	0.181±0.017	0.55	46.7±1.6	0.206±0.007	0.65	49.5±1.5	0.217±0.004
0.75	52.0±1.5	0.229±0.004	0.85	51.6±1.3	0.229±0.006	0.95	53.7±1.2	0.253±0.006
1.05	55.9±1.2	0.264±0.007	1.15	55.6±1.2	0.293±0.007	1.25	52.6±1.3	0.313±0.009
				E_{ZCAL} class 3, $\mathrm{mult}_{\mathrm{NMA}}$ class 2				
0.45	44.1±1.6	0.169±0.016	0.55	46.4±1.5	0.210±0.007	0.65	48.2±1.5	0.217±0.004
0.75	46.6±1.4	0.230±0.004	0.85	48.2±1.2	0.240±0.007	0.95	49.0±1.1	0.269±0.007
1.05	47.8±1.1	0.274±0.008	1.15	48.1±1.1	0.296±0.007	1.25	50.9±1.4	0.288±0.008
				E_{ZCAL} class 3, $\mathrm{mult}_{\mathrm{NMA}}$ class 3				
0.45	41.0±1.4	0.204±0.020	0.55	44.5±1.5	0.203±0.007	0.65	42.9±1.3	0.212±0.004
0.75	41.6±1.2	0.226±0.004	0.85	42.7±1.1	0.234±0.006	0.95	42.9±1.0	0.259±0.008
1.05	44.5±1.1	0.250±0.007	1.15	44.3±1.1	0.275±0.007	1.25	45.1±1.3	0.285±0.008

=1.6. For a given E_{ZCAL} cut, the rms value of the proton dN/dy distribution decreases with increasing multiplicity.

The rms value of the proton distributions (Fig. 8) are similar in shape if the NMA multiplicity is the same, even for different values of E_{ZCAL} (Fig. 5). This can also be observed by proceeding diagonally up from left to right in Fig. 7. The proton rapidity distribution in the lowest $\mathrm{mult}_{\mathrm{NMA}}$ cut for the most central E_{ZCAL} is similar to the proton distribution from the middle $\mathrm{mult}_{\mathrm{NMA}}$ cut for the more peripheral E_{ZCAL}.

The correlation between event multiplicity and the width of the proton dN/dy is consistent with the following hypothesis. In reactions of similar initial geometry that stochastically have a larger average rapidity loss per nucleon, more energy is deposited into the collision zone, which leads to greater particle production and higher event multiplicity. The event class with the narrowest proton dN/dy (low E_{ZCAL} and highest $\mathrm{mult}_{\mathrm{NMA}}$) could therefore contain an enriched sample of events with a large volume of the most dense matter.

The proton dN/dy distribution from the most geometrically central, highest multiplicity event class was fitted with a Gaussian distribution. The fitted width was $\sigma = 1.19 \pm 0.05$. This is narrower than the width of the proton distribution [7] in central Au+Au collisions solely selected on E_{ZCAL}, where the fitted width is $\sigma = 1.28 \pm 0.03$.

In contrast to the dN/dy distributions, the mean m_t for protons (Table IV) show little change as a function of $\mathrm{mult}_{\mathrm{NMA}}$ for a given E_{ZCAL}. This is discussed further in Sec. VI along with mean m_t for pions.

V. PARTICLE PRODUCTION

To probe the relation between the energy deposited in a system and the yields of produced particles, the spectra and

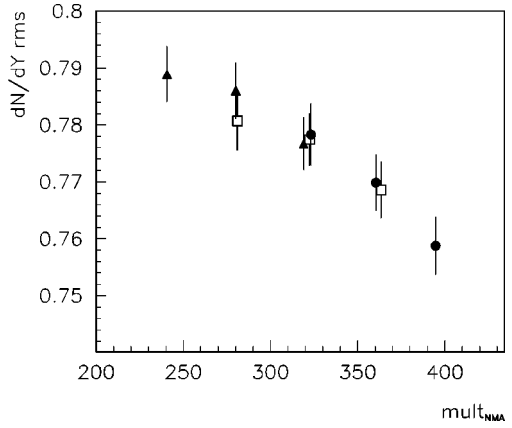

FIG. 8. The restricted rms of proton dN/dy distributions from Au+Au reactions at 11.6*A* GeV/c are plotted versus mult$_{\mathrm{NMA}}$ for each event class doubly selected on mult$_{\mathrm{NMA}}$ and E_{ZCAL} (Table III). The proton rms for the 0–3 % E_{ZCAL} range of events is shown as filled circles, the 3–7 % range is shown as open squares while the 7–12 % range is shown as filled triangles.

yields of π^+ and K^+ have been measured as a function of both global event characteristics, E_{ZCAL} and mult$_{\mathrm{NMA}}$. To understand the features of particle production in doubly-selected event classes, it is useful to first study particle production as a function of one of the global observables, E_{ZCAL}. Previous publications from our collaboration have presented the pion spectra and yields from central collisions [7] and the dependence of K^+ yields on E_{ZCAL} [9].

Figure 9 plots the invariant transverse spectra of π^+ as a function of transverse mass for the geometrically most central reactions solely selected on E_{ZCAL} (Table II). At low m_t these spectra rise above an exponential function. The spectra are well fit by a scaled exponential function

$$\frac{1}{2\pi m_t}\frac{d^2N}{dm_t dy}=\frac{dN/dy}{2\pi T_s^{2-\lambda}\Gamma(2-\lambda,m_0/T_s)}m_t^{-\lambda}e^{-m_t/T_s}, \tag{10}$$

where $\Gamma(2-\lambda,m_0/T_s)$, the complementary incomplete gamma function, is introduced into the normalization so that dN/dy is a fitted parameter. The other two parameters are λ and T_s. To compare the pion and proton transverse spectra, the mean m_t, is calculated

$$\langle m_t\rangle=\frac{T_s\Gamma(3-\lambda,m_0/T_s)}{\Gamma(2-\lambda,m_0/T_s)}. \tag{11}$$

The transverse spectra can also be fit with a sum of two exponentials. This produced dN/dy and $\langle m_t\rangle$ values within 5% of the values from the scaled exponential fit. The scaled exponential fits to the pion transverse spectra will be used throughout this paper.

The dN/dy distributions of π^+ from central events selected solely on E_{ZCAL} are shown in Fig. 10 and tabulated in Table V for each E_{ZCAL} class of Table II. The dN/dy distributions of π^+ increase as the reactions become more central.

The kaon transverse spectra from central events selected solely on E_{ZCAL} are shown in Fig. 11 and are well fit with a single exponential function

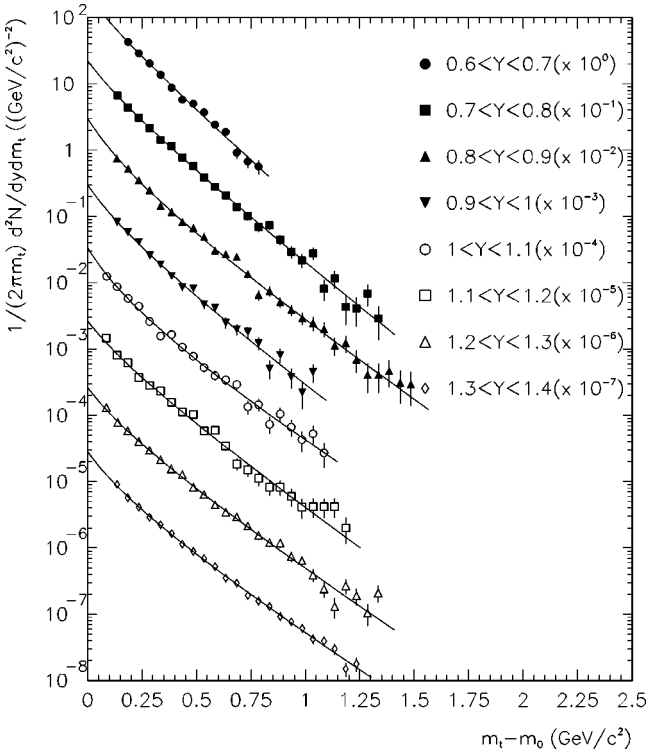

FIG. 9. The invariant spectra for π^+ from Au+Au reactions at 11.6*A* GeV/c for different slices in rapidity from the most central event class (0–3 % Table II) solely selected on E_{ZCAL}. The lines are fits to the data with the scaled exponential functional form [Eq. (10)].

$$\frac{1}{2\pi m_t}\frac{d^2N}{dm_t dy}=\frac{dN/dy}{2\pi(T_E m_0+T_E^2)}e^{-(m_t-m_0)/T_E}. \tag{12}$$

The fitted parameters are the dN/dy and inverse slope, T_E. The kaon mean m_t values are calculated

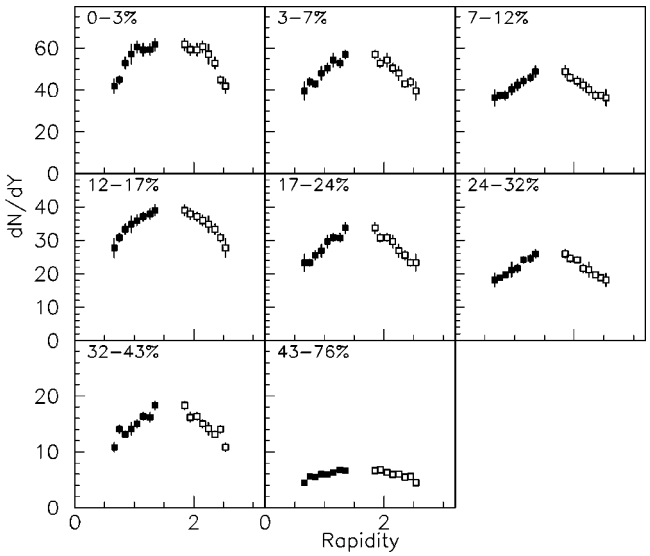

FIG. 10. The $\pi^+ dN/dy$ distribution from Au+Au reactions at 11.6*A* GeV/c for each event class determined solely by E_{ZCAL}, Table II. The open points are the data reflected about midrapidity.

TABLE V. The $\pi^+ dN/dy$ and $\langle m_t\rangle - m_0$ distributions in Au+Au reactions at 11.6A GeV/c for each event class solely selected on E_{ZCAL} (Table II).

y	dN/dy	$\langle m_t\rangle - m_0$	y	dN/dy	$\langle m_t\rangle - m_0$
		E_{ZCAL} class 1			
0.66	41.8±3.6	0.193±0.011	0.75	45.0±2.0	0.208±0.009
0.84	52.6±2.9	0.206±0.011	0.95	57.1±4.8	0.209±0.014
1.05	60.7±2.9	0.218±0.067	1.15	59.3±2.4	0.230±0.008
1.26	59.3±2.9	0.240±0.010	1.35	61.7±2.9	0.239±0.009
		E_{ZCAL} class 2			
0.66	39.6±4.5	0.187±0.008	0.75	43.9±2.2	0.195±0.007
0.84	42.9±1.7	0.217±0.009	0.95	48.0±3.5	0.202±0.014
1.05	50.4±2.4	0.212±0.011	1.15	54.3±3.3	0.221±0.011
1.26	52.9±2.3	0.233±0.009	1.35	56.9±2.1	0.234±0.008
		E_{ZCAL} class 3			
0.66	36.3±4.1	0.186±0.012	0.75	37.4±1.7	0.197±0.009
0.84	37.4±2.2	0.209±0.009	0.95	40.1±2.8	0.217±0.014
1.05	42.4±2.8	0.212±0.012	1.15	44.2±2.4	0.222±0.011
1.26	46.0±2.1	0.233±0.009	1.35	48.8±2.9	0.226±0.010
		E_{ZCAL} class 4			
0.66	27.7±2.9	0.194±0.013	0.75	30.8±1.4	0.198±0.008
0.84	33.3±1.7	0.200±0.010	0.95	34.7±2.6	0.204±0.014
1.05	35.9±1.7	0.214±0.011	1.15	37.0±1.4	0.219±0.010
1.26	37.8±1.7	0.231±0.009	1.35	39.0±1.7	0.229±0.008
		E_{ZCAL} class 5			
0.66	23.3±2.7	0.183±0.031	0.75	23.3±1.0	0.202±0.011
0.84	25.5±1.4	0.201±0.012	0.95	26.9±2.1	0.211±0.060
1.05	29.6±2.0	0.204±0.019	1.15	30.9±1.2	0.212±0.063
1.26	30.7±1.4	0.229±0.021	1.35	33.6±1.8	0.220±0.031
		E_{ZCAL} class 6			
0.66	18.2±2.0	0.186±0.008	0.75	18.9±0.9	0.201±0.009
0.84	19.7±1.0	0.206±0.009	0.95	21.2±2.3	0.196±0.017
1.05	21.6±1.3	0.213±0.012	1.15	24.1±1.1	0.208±0.006
1.26	24.5±1.2	0.216±0.009	1.35	26.0±1.3	0.215±0.008
		E_{ZCAL} class 7			
0.66	10.8±0.8	0.193±0.010	0.75	14.1±0.7	0.182±0.008
0.84	13.1±0.6	0.209±0.010	0.95	14.1±1.2	0.203±0.017
1.05	15.0±0.8	0.198±0.012	1.15	16.4±0.7	0.203±0.009
1.26	16.2±0.9	0.220±0.010	1.35	18.3±0.8	0.211±0.006
		E_{zCAL} class 8			
0.66	4.5±0.3	0.186±0.010	0.75	5.6±0.3	0.179±0.008
0.85	5.5±0.3	0.192±0.010	0.95	6.0±0.6	0.187±0.014
1.05	6.0±0.4	0.197±0.011	1.15	6.3±0.3	0.194±0.011
1.26	6.8±0.3	0.205±0.009	1.35	6.7±0.2	0.214±0.007

$$\langle m_t\rangle = \frac{m_0^2 + 2m_0T_E + 2T_E^2}{m_0 + T_E}. \tag{13}$$

$$\text{fiducial yield} = \sum \frac{dN}{dy}dy. \tag{14}$$

The kaon dN/dy distributions for each E_{ZCAL} class (Table II) are shown in Fig. 12 and tabulated in Table VI.

The dN/dy distributions for pions and kaons do not cover the midrapidity region, nor do they extend to target rapidity. The total yield can be estimated by fitting these distributions to Gaussians and integrating to obtain the π^+ and K^+ total yields. However, there is an extra systematic uncertainty from this extrapolation. Instead a fiducial yield is used throughout this paper, where

For dN/dy distributions selected on E_{ZCAL}, the sum in the fiducial yield runs between $0.6<y<1.3$.

In Fig. 13 the fiducial yields of π^+ and K^+ are plotted versus the average number of projectile participants, N_{pp}, for that event class. The fiducial yields are tabulated in Table VII. These yields increase nonlinearly with N_{pp}, especially for kaons. The nonlinear increase implies that particle production is enhanced in central reactions.

This is emphasized in Fig. 14, where the yield of kaons and pions per participant is plotted versus N_{pp}. The yield per

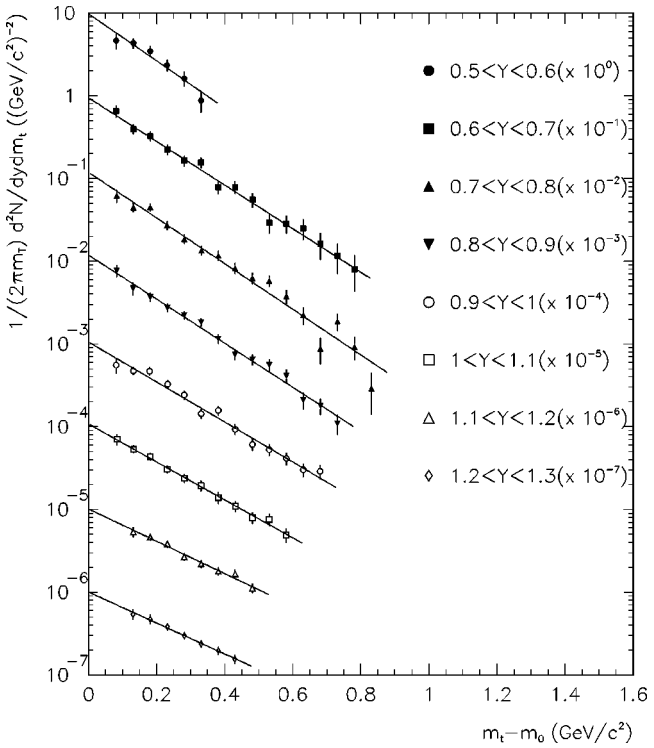

FIG. 11. The invariant spectra for K^+ from Au+Au reactions at 11.6*A* GeV/*c* for different slices in rapidity from the most central event class (0–3 % Table II) solely selected on E_{ZCAL}. The lines are fits to the data with the exponential functional form [Eq. (12)].

participant for pions is flatter in midperipheral collisions than for kaons. The π^+ fiducial yield per participant increases more strongly in the last three centrality classes. This increase in fiducial yield could be driven by either a change in the shape of the pion rapidity distribution or an overall increase in the pion yield. To test for a change in the shape of the rapidity distribution, the restricted dN/dy_{rms} [Eq. (9) calculated between $0.6<y<1.3$] for the $\pi^+ dN/dy$ distributions

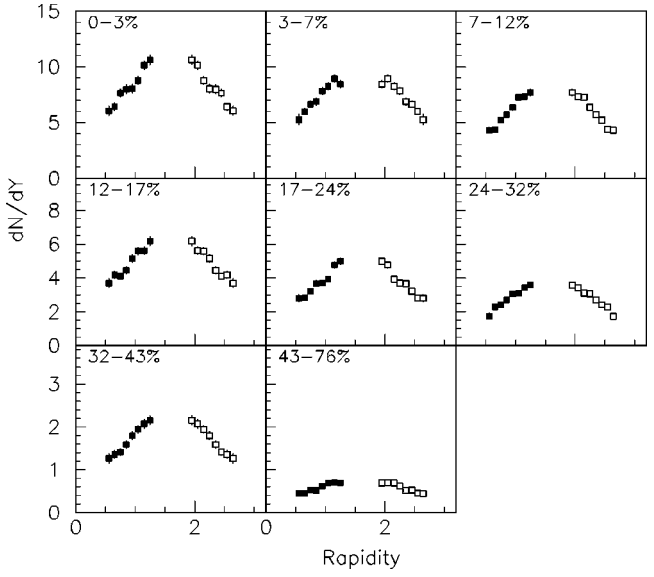

FIG. 12. The K^+dN/dy distribution from Au+Au reactions at 11.6*A* GeV/*c* for each event class determined solely by E_{ZCAL}, Table II. The open points are the data reflected about midrapidity.

is plotted in Fig. 15 as a function of N_{pp}. The rms value is independent of centrality, which implies that the change in pion fiducial yields is driven largely by an increase in overall pion production.

The ratio of the fiducial yields, K^+/π^+, is plotted versus N_{pp} in Fig. 16. The ratio increases smoothly from peripheral reactions to central collisions and appears to reach a plateau of K^+/π^+ of 0.16 in central reactions. This ratio of fiducial yields covers the phase space $0.6<y<1.3$. In this region the K^+/π^+ ratio is lower than the midrapidity K^+/π^+ ratio of 0.19 [9]. The K^+/π^+ ratio for each centrality class is larger than the ratio from isospin-averaged *N*-*N* collisions at the same beam energy [9,13,14] (Fig. 16).

To understand the evolution of K^+/π^+ with centrality, it is best to reexamine how the yields of π^+ and K^+ varied with N_{pp} (Fig. 13). In the peripheral reactions the pion yield increases with N_{pp}, however the K^+ yield increases with N_{pp} at a greater, nonlinear rate. Hence the K^+/π^+ ratio increases. For more central reactions both the π^+ and K^+ yields show a similar nonlinear increase with N_{pp}, and the K^+/π^+ ratio appears to plateau.

VI. PARTICLE PRODUCTION IN DOUBLY SELECTED EVENTS

Recall that in Secs. III and IV, events were studied in a two-dimensional grid of global event characteristics, E_{ZCAL} and $\mathrm{mult}_{\mathrm{NMA}}$. The proton dN/dy distributions for each event class were presented in Sec. IV. These events can be further characterized by the proton mean m_t, the produced particle spectra and the relative production of strange and nonstrange mesons.

The dN/dy distributions of π^+ and K^+ are plotted in Figs. 17 and 18 for the grid of double cuts in E_{ZCAL} and in $\mathrm{mult}_{\mathrm{NMA}}$ (Table III). These dN/dy distributions are tabulated in Tables VIII and IX. For a given range of E_{ZCAL}, the yields of π^+ and K^+ trivially increase with multiplicity since the yields in the spectrometer must track the event multiplicity.

The π^+ and $K^+ dN/dy$ distributions are summed over a limited range of rapidity, $0.6<y<1.2$, to form a fiducial yield. Because the rapidity bins used in the double-event class are $\Delta y=0.2$, the rapidity range for the fiducial yield is slightly narrower than was used to calculate the fiducial yield for events solely selected on E_{ZCAL}.

The fiducial yields for doubly-selected pions and kaons are tabulated in Table X. Figure 19 shows the ratio of fiducial yields K^+/π^+ versus multiplicity for each of the three most central E_{ZCAL} cuts (Table III). In Sec. V the K^+/π^+ ratio was shown to be independent of E_{ZCAL} over this range of centrality. Extending this, Fig. 19 shows that the ratio K^+/π^+ does not depend on multiplicity for a given E_{ZCAL} cut. Even though the incoming baryons lose more rapidity and the total number of produced particles increases, there is no increase in the fraction of strange particles.

For several years it has been observed [15,16] that the transverse spectra for heavy particles are harder than for light particles. This is consistent with an expansion increasing the transverse spectra of all particles but affecting most the momentum of the heavier particles. The mean m_t, $\langle m_t \rangle$, can be used to characterize the transverse spectra of both pions and

TABLE VI. The $K^+ dN/dy$ and $\langle m_t \rangle - m_0$ distributions in Au+Au reactions at 11.6A GeV/c for each event class solely selected on E_{ZCAL} (Table II).

y	dN/dy	$\langle m_t \rangle - m_0$	y	dN/dy	$\langle m_t \rangle - m_0$
		E_{ZCAL} class 1			
0.55	6.05±0.44	0.189±0.029	0.65	6.42±0.36	0.206±0.011
0.75	7.65±0.38	0.196±0.007	0.85	7.98±0.42	0.204±0.009
0.95	8.03±0.39	0.228±0.011	1.05	8.76±0.37	0.242±0.015
1.15	10.14±0.41	0.292±0.029	1.25	10.63±0.45	0.306±0.038
		E_{ZCAL} class 2			
0.55	5.26±0.49	0.265±0.058	0.65	5.98±0.31	0.196±0.008
0.75	6.62±0.31	0.197±0.007	0.85	6.88±0.33	0.218±0.010
0.95	7.83±0.34	0.232±0.011	1.05	8.25±0.33	0.220±0.012
1.15	8.94±0.34	0.281±0.025	1.25	8.45±0.35	0.261±0.029
		E_{ZCAL} class 3			
0.55	4.31±0.31	0.180±0.026	0.65	4.36±0.24	0.215±0.012
0.75	5.23±0.25	0.224±0.010	0.85	5.71±0.28	0.220±0.010
0.95	6.36±0.28	0.226±0.010	1.05	7.28±0.28	0.234±0.013
1.15	7.32±0.29	0.255±0.021	1.25	7.70±0.30	0.276±0.028
		E_{ZCAL} class 4			
0.55	3.68±0.27	0.165±0.024	0.65	4.19±0.23	0.190±0.009
0.75	4.11±0.20	0.204±0.008	0.85	4.45±0.23	0.215±0.010
0.95	5.15±0.24	0.214±0.010	1.05	5.59±0.23	0.224±0.012
1.15	5.61±0.23	0.250±0.021	1.25	6.18±0.29	0.338±0.047
		E_{ZCAL} class 5			
0.55	2.80±0.21	0.187±0.030	0.65	2.81±0.16	0.200±0.010
0.75	3.22±0.17	0.205±0.009	0.85	3.66±0.19	0.212±0.010
0.95	3.71±0.18	0.216±0.010	1.05	3.93±0.17	0.225±0.015
1.15	4.76±0.20	0.241±0.019	1.25	4.98±0.20	0.295±0.035
		E_{ZCAL} class 6			
0.55	1.73±0.20	0.255±0.078	0.65	2.28±0.14	0.186±0.009
0.75	2.42±0.13	0.210±0.009	0.85	2.69±0.15	0.197±0.009
0.95	3.06±0.15	0.211±0.010	1.05	3.09±0.14	0.201±0.010
1.15	3.42±0.16	0.234±0.020	1.25	3.57±0.15	0.288±0.035
		E_{ZCAL} class 7			
0.55	1.27±0.12	0.144±0.024	0.65	1.36±0.09	0.174±0.011
0.75	1.41±0.08	0.204±0.009	0.85	1.59±0.09	0.209±0.011
0.95	1.80±0.10	0.198±0.010	1.05	1.94±0.09	0.208±0.012
1.15	2.07±0.11	0.211±0.018	1.25	2.15±0.11	0.225±0.021
		E_{ZCAL} class 8			
0.55	0.44±0.04	0.149±0.026	0.65	0.45±0.03	0.176±0.010
0.75	0.52±0.03	0.176±0.008	0.85	0.52±0.03	0.186±0.009
0.95	0.62±0.04	0.167±0.008	1.05	0.69±0.04	0.168±0.009
1.15	0.70±0.04	0.200±0.016	1.25	0.69±0.03	0.245±0.029

protons. This is representative of the whole spectrum as compared to using the inverse slope of high momentum particles [16].

For events doubly selected on E_{ZCAL} and $\mathrm{mult}_{\mathrm{NMA}}$, $\langle m_t \rangle$ is plotted versus rapidity in Fig. 20 for protons and in Fig. 21 for pions. The rest mass m_0 is subtracted to remove the trivial mass difference between pions and protons. The protons have a strong increase of $\langle m_t \rangle$ towards midrapidity. The pion $\langle m_t \rangle$ distribution also increases but the dependence on rapidity is less strong. The $\langle m_t \rangle$ distributions for both protons and pions show little change as a function of event class. The $\langle m_t \rangle$ distributions for K^+ are tabulated in Table VI.

The change in the $\langle m_t \rangle$ distributions as a function of event class can be examined by calculating the fiducial average of $\langle m_t \rangle$ for protons and pions over a common range of rapidity,

TABLE VII. The fiducial yields for π^+ and K^+ for each event class selected solely on E_{ZCAL}.

E_{ZCAL} class	π^+ fiducial yield	K^+ fiducial yield
0–3 %	37.63± 0.91	5.97± 0.11
3–7 %	32.92± 0.63	5.30± 0.09
7–12 %	28.28± 0.56	4.40± 0.07
12–17 %	23.29± 0.45	3.53± 0.06
17–24 %	18.87± 0.38	2.71± 0.05
24–32 %	14.55± 0.32	2.05± 0.04
32–43 %	9.72± 0.22	1.23± 0.03
43–76 %	3.98± 0.09	0.42± 0.01

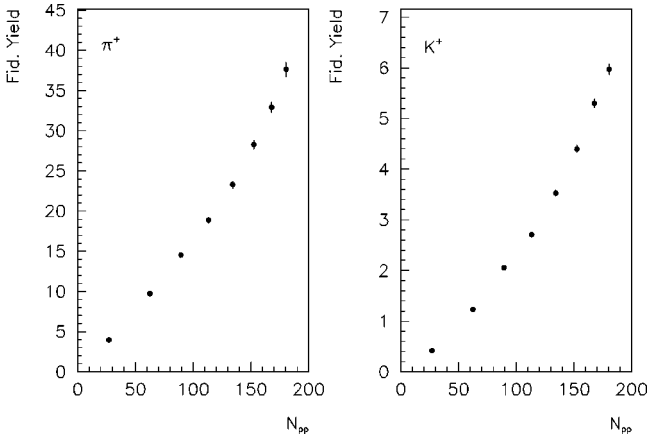

FIG. 13. The fiducial yields for π^+, K^+ from Au+Au reactions at 11.6*A* GeV/*c* plotted as a function of N_{pp}.

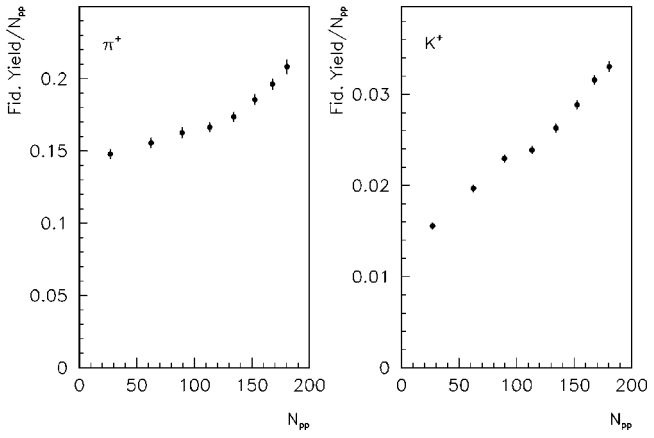

FIG. 14. The fiducial yields per projectile participant for π^+, K^+ from Au+Au reactions at 11.6*A* GeV/*c* plotted as a function of N_{pp}.

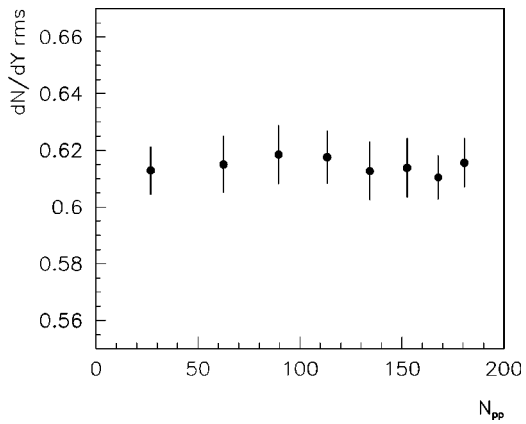

FIG. 15. The restricted rms of the $\pi^+ dN/dy$ distribution from Au+Au reactions at 11.6*A* GeV/*c* plotted as a function of N_{pp}.

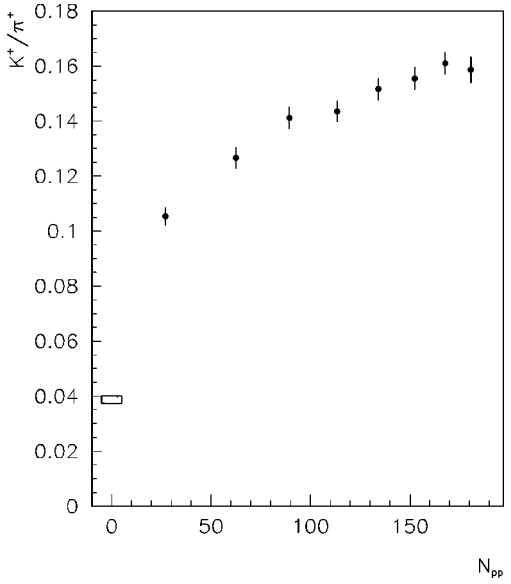

FIG. 16. The ratio of fiducial yields K^+/π^+ from Au+Au reactions at 11.6*A* GeV/*c* plotted versus N_{pp}. The box at N_{pp} is the K^+/π^+ ratio over full phase space from isospin-averaged *N*-*N* collisions at the same beam energy [9].

$$\overline{\langle m_t \rangle} = \frac{\sum \langle m_t \rangle dN/dy}{\sum dN/dy} \tag{15}$$

between $0.6 < y < 1.4$.

The $\langle m_t \rangle - m_0$ for pions and protons is plotted for each event class doubly selected on E_{ZCAL} and $\mathrm{mult}_{\mathrm{NMA}}$ in Fig.

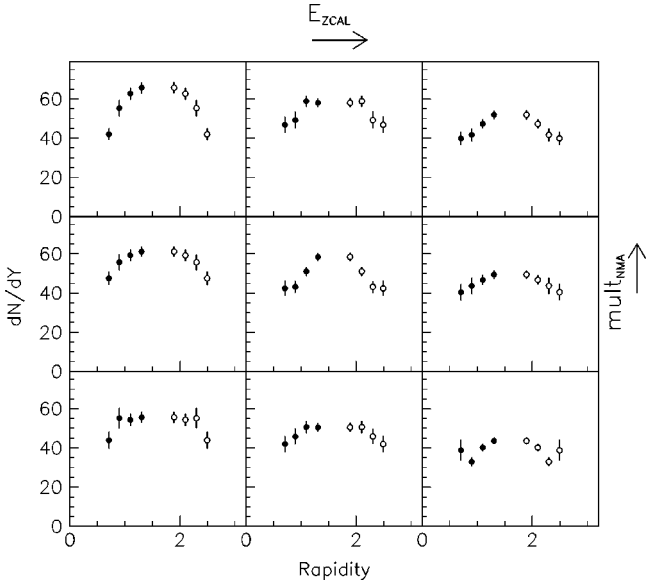

FIG. 17. The $\pi^+ dN/dy$ distributions from Au+Au reactions at 11.6*A* GeV/*c* are plotted for the most central E_{ZCAL} cuts divided into three $\mathrm{mult}_{\mathrm{NMA}}$ regions (Table III). Each column corresponds to a range in E_{ZCAL} with the most geometrically central events in the left column. For a given E_{ZCAL}, the multiplicity increases from bottom to top. The open points are the data reflected about midrapidity.

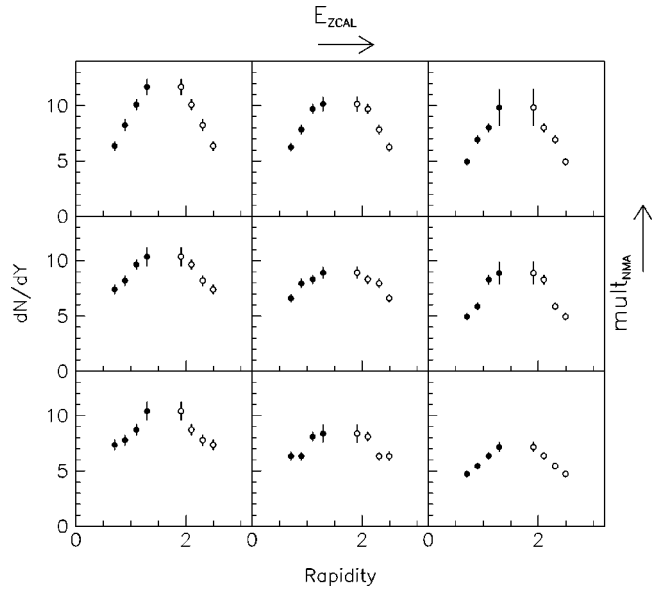

FIG. 18. The $K^+ dN/dy$ distributions from Au+Au reactions at 11.6A GeV/c are plotted for the most central E_{ZCAL} cuts divided into three $\mathrm{mult}_{\mathrm{NMA}}$ regions (Table III). Each column corresponds to a range in E_{ZCAL} with the most geometrically central events in the left column. For a given E_{ZCAL}, the multiplicity increases from bottom to to top. The open points are the data reflected about midrapidity.

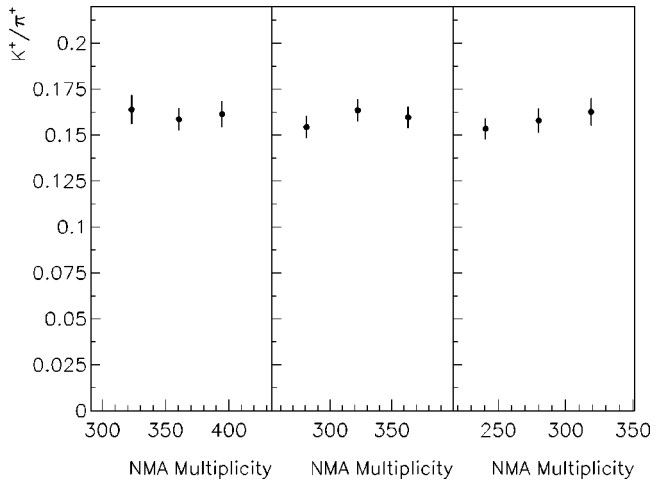

FIG. 19. The fiducial K^+/π^+ from Au+Au reactions at 11.6A GeV/c for events doubly selected on $\mathrm{mult}_{\mathrm{NMA}}$ and E_{ZCAL}. Each panel corresponds to a range in E_{ZCAL} (left panel 0–3 %, middle panel 3–7 %, right panel 7–12% of the interaction cross section). Within each panel the K^+/π^+ ratio is plotted versus the NMA multiplicity.

TABLE VIII. The dN/dy and $\langle m_t\rangle - m_0$ distributions for π^+ in Au+Au reactions at 11.6A GeV/c for each event class doubly selected on E_{ZCAL} and $\mathrm{mult}_{\mathrm{NMA}}$ (Table III).

y	dN/dy	$\langle m_t\rangle - m_0$	y	dN/dy	$\langle m_t\rangle - m_0$
		E_{ZCAL} class 1, $\mathrm{mult}_{\mathrm{NMA}}$ class 1			
0.71	42.0±3.0	0.202±0.011	0.90	55.3±4.1	0.206±0.012
1.10	62.7±3.0	0.225±0.008	1.31	65.7±2.8	0.236±0.010
		E_{ZCAL} class 1, $\mathrm{mult}_{\mathrm{NMA}}$ class 2			
0.71	47.5±3.4	0.193±0.010	0.90	55.7±4.1	0.208±0.012
1.10	59.3±3.0	0.223±0.007	1.31	61.2±2.6	0.245±0.007
		E_{ZCAL} class 1, $\mathrm{mult}_{\mathrm{NMA}}$ class 3			
0.71	43.9±4.3	0.208±0.034	0.90	55.1±5.1	0.200±0.013
1.10	54.3±3.0	0.217±0.011	1.31	55.6±2.9	0.238±0.010
		E_{ZCAL} class 2, $\mathrm{mult}_{\mathrm{NMA}}$ class 1			
0.71	46.8±4.1	0.185±0.008	0.90	49.3±4.3	0.203±0.011
1.10	58.8±2.8	0.219±0.008	1.31	58.1±2.3	0.241±0.007
		E_{ZCAL} class 2, $\mathrm{mult}_{\mathrm{NMA}}$ class 2			
0.71	42.5±3.7	0.193±0.008	0.90	43.1±3.0	0.218±0.012
1.10	51.0±2.3	0.222±0.008	1.31	58.5±2.1	0.228±0.007
		E_{ZCAL} class 2, $\mathrm{mult}_{\mathrm{NMA}}$ class 3			
0.71	41.9±4.1	0.188±0.009	0.90	45.8±4.0	0.201±0.012
1.10	50.7±3.1	0.199±0.010	1.31	50.5±2.3	0.228±0.009
		E_{ZCAL} class 3, $\mathrm{mult}_{\mathrm{NMA}}$ class 1			
0.71	39.9±3.3	0.193±0.008	0.90	41.7±3.2	0.217±0.014
1.10	47.3±2.3	0.212±0.007	1.31	51.9±2.3	0.231±0.008
		E_{ZCAL} class 3, $\mathrm{mult}_{\mathrm{NMA}}$ class 2			
0.71	40.4±4.2	0.185±0.011	0.90	43.7±4.2	0.195±0.013
1.10	46.7±2.5	0.207±0.008	1.31	49.4±2.2	0.226±0.007
		E_{ZCAL} class 3, $\mathrm{mult}_{\mathrm{NMA}}$ class 3			
0.71	38.8±5.2	0.184±0.014	0.90	33.0±2.2	0.221±0.012
1.10	40.3±1.9	0.228±0.008	1.31	43.6±1.7	0.221±0.008

TABLE IX. The dN/dy and $\langle m_t\rangle - m_0$ distributions for K^+ in Au+Au reactions at 11.6A GeV/c for each event class doubly selected on E_{ZCAL} and $\mathrm{mult}_{\mathrm{NMA}}$ (Table III).

y	dN/dy	$\langle m_t\rangle - m_0$	y	dN/dy	$\langle m_t\rangle - m_0$
		E_{ZCAL} class 1, $\mathrm{mult}_{\mathrm{NMA}}$ class 1			
0.71	6.35±0.42	0.198±0.012	0.89	8.25±0.52	0.205±0.012
1.10	10.09±0.49	0.269±0.029	1.29	11.68±0.71	0.264±0.075
		E_{ZCAL} class 1, $\mathrm{mult}_{\mathrm{NMA}}$ class 2			
0.70	7.39±0.43	0.211±0.011	0.89	8.18±0.47	0.223±0.013
1.10	9.66±0.46	0.282±0.033	1.29	10.35±0.84	0.308±0.103
		E_{ZCAL} class 1, $\mathrm{mult}_{\mathrm{NMA}}$ class 3			
0.71	7.35±0.45	0.221±0.012	0.89	7.77±0.47	0.227±0.013
1.10	8.71±0.48	0.249±0.026	1.29	10.40±0.83	0.229±0.058
		E_{ZCAL} class 2, $\mathrm{mult}_{\mathrm{NMA}}$ class 1			
0.71	6.24±0.38	0.000±0.000	0.89	7.84±0.43	0.000±0.000
1.10	9.71±0.45	0.000±0.000	1.29	10.14±0.64	0.000±0.000
		E_{ZCAL} class 2, $\mathrm{mult}_{\mathrm{NMA}}$ class 2			
0.71	6.59±0.36	0.000±0.000	0.89	7.95±0.42	0.000±0.000
1.10	8.30±0.39	0.000±0.000	1.29	8.90±0.51	0.000±0.000
		E_{ZCAL} class 2, $\mathrm{mult}_{\mathrm{NMA}}$ class 3			
0.71	6.34±0.39	0.000±0.000	0.89	6.31±0.36	0.000±0.000
1.10	8.10±0.40	0.000±0.000	1.29	8.37±0.79	0.000±0.000
		E_{ZCAL} class 3, $\mathrm{mult}_{\mathrm{NMA}}$ class 1			
0.71	4.93±0.30	0.000±0.000	0.89	6.94±0.37	0.000±0.000
1.10	8.00±0.39	0.000±0.000	1.29	9.84±1.65	0.000±0.000
		E_{ZCAL} class 3, $\mathrm{mult}_{\mathrm{NMA}}$ class 2			
0.71	4.95±0.30	0.000±0.000	0.89	5.87±0.34	0.000±0.000
1.10	8.28±0.43	0.000±0.000	1.29	8.88±1.00	0.000±0.000
		E_{ZCAL} class 3, $\mathrm{mult}_{\mathrm{NMA}}$ class 3			
0.71	4.72±0.29	0.000±0.000	0.89	5.44±0.30	0.000±0.000
1.10	6.35±0.32	0.000±0.000	1.29	7.16±0.45	0.000±0.000

22. The $\langle m_t\rangle - m_0$ for protons is larger than for pions, consistent with transverse expansion of the system. The values of $\langle m_t\rangle - m_0$ for both pions and protons increase slightly in the most geometrically central event class (lowest E_{ZCAL}). There are however no consistent trends in the difference between $\langle m_t\rangle - m_0$ for protons and pions, indicating little or no change in the expansion for different event classes.

TABLE X. The fiducial yields for π^+ and K^+ in Au+Au reactions at 11.6A GeV/c for each event class doubly selected on E_{ZCAL} and $\mathrm{mult}_{\mathrm{NMA}}$ (Table III).

Event class	π^+ fiducial yield	K^+ fiducial yield
E_{ZCAL} 1 $\mathrm{mult}_{\mathrm{NMA}}$ 1	45.2±1.4	7.29±0.22
E_{ZCAL} 1 $\mathrm{mult}_{\mathrm{NMA}}$ 2	44.4±1.2	7.04±0.19
E_{ZCAL} 1 $\mathrm{mult}_{\mathrm{NMA}}$ 3	41.3±1.1	6.76±0.26
E_{ZCAL} 2 $\mathrm{mult}_{\mathrm{NMA}}$ 1	42.1±1.1	6.72±0.18
E_{ZCAL} 2 $\mathrm{mult}_{\mathrm{NMA}}$ 2	38.7±0.9	6.33±0.17
E_{ZCAL} 2 $\mathrm{mult}_{\mathrm{NMA}}$ 3	37.2±1.0	5.74±0.17
E_{ZCAL} 3 $\mathrm{mult}_{\mathrm{NMA}}$ 1	35.7±0.9	5.80±0.22
E_{ZCAL} 3 $\mathrm{mult}_{\mathrm{NMA}}$ 2	35.0±0.9	5.53±0.18
E_{ZCAL} 3 $\mathrm{mult}_{\mathrm{NMA}}$ 3	30.8±0.7	4.72±0.13

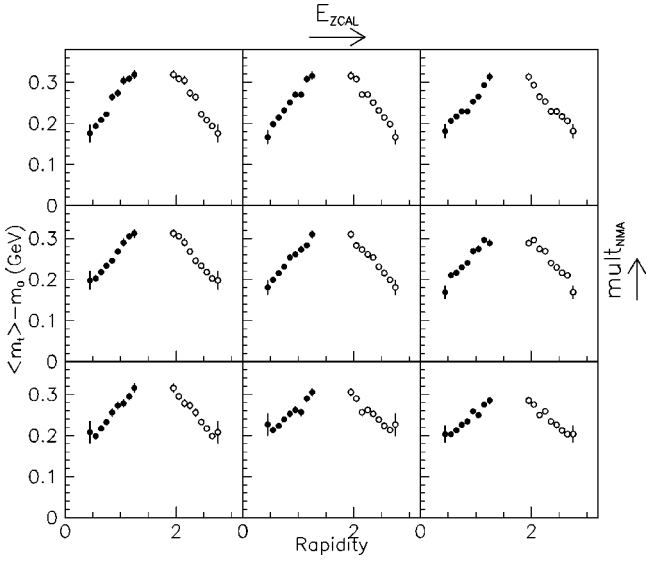

FIG. 20. The proton $\langle m_t\rangle - m_0$ versus rapidity from Au+Au reactions at 11.6A GeV/c are plotted for event class doubly selected on $\mathrm{mult}_{\mathrm{NMA}}$ and E_{ZCAL} (Table III). Each column corresponds to a range in E_{ZCAL} with the most geometrically central events in the left column. For a given E_{ZCAL}, the multiplicity increases from bottom to top. The open points are the data reflected about midrapidity.

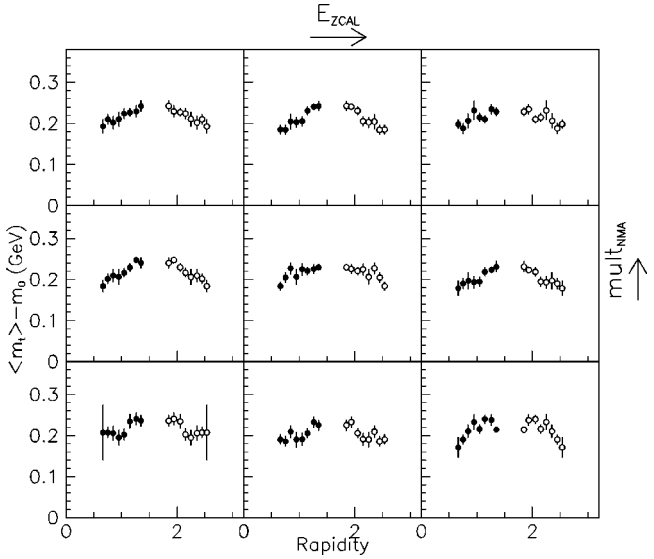

FIG. 21. The pion $\langle m_t \rangle - m_0$ versus rapidity from Au+Au reactions at 11.6A GeV/c are plotted for event class doubly selected on mult_{NMA} and E_{ZCAL} (Table III). Each column corresponds to a range in E_{ZCAL} with the most geometrically central events in the left column. For a given E_{ZCAL}, the multiplicity increases from bottom to top. The open points are the data reflected about midrapidity.

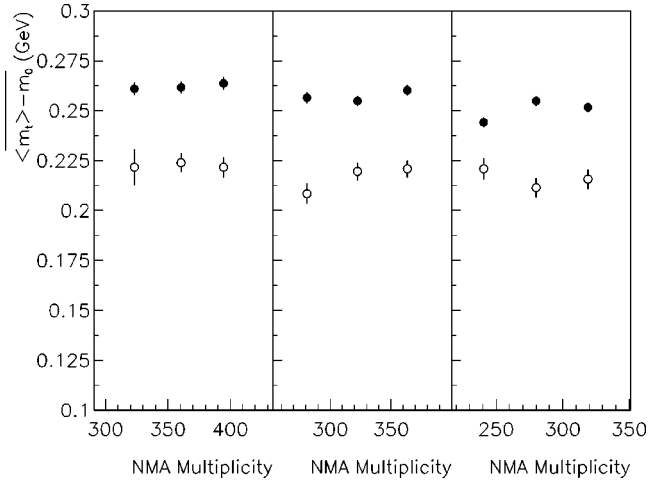

FIG. 22. The fiducial average of $\langle m_t \rangle - m_0$ for protons (filled circles) and π^+ (open circles) from Au+Au reactions at 11.6A GeV/c for events doubly selected on mult_{NMA} and E_{ZCAL}. Each panel corresponds to a range in E_{ZCAL} (left panel 0–3 %, middle panel 3–7 %, right panel 7–12 % of the interaction cross section). Within each panel the fiducial average of $\langle m_t \rangle - m_0$ is plotted versus the NMA multiplicity.

VII. CONCLUSIONS

Events from Au+Au collisions at 11.6A GeV/c have been selected in a two-dimensional grid of two global observables, the energy near zero degrees, E_{ZCAL}, and the multiplicity, mult_{NMA}. Though both E_{ZCAL} and mult_{NMA} are sensitive to the collision centrality, they are not the same measure. E_{ZCAL} provides an estimate of the number of projectile participants, mult_{NMA} is sensitive to the full evolution of the reaction including the many secondary hadron-hadron collisions in the participant zone.

The two global observables, mult_{NMA} and E_{ZCAL}, are correlated (Fig. 5) with a significant width to the correlation. The average multiplicity increases nonlinearly with decreasing values of E_{ZCAL}, similar to the observation in Si+A reactions [2]. There is no indication of the predicted shoulder or extra group of rare high multiplicity events [6].

For moderately central reactions ($\sigma/\sigma_{\text{int}} < 12\%$) the proton rapidity distributions do not depend on E_{ZCAL} but only on the event multiplicity. The hypothesis is made that for events with a larger average rapidity loss per nucleon, more energy is deposited into the collision zone, which leads to greater particle production and higher event multiplicity. In contrast to the change of proton dN/dy, the shape of the proton transverse spectra, over the measured rapidity range, shows little dependence on the event multiplicity.

The event class with the lowest E_{ZCAL} and the highest event multiplicity has the narrowest proton dN/dy distribution and hence could contain an enriched sample of events with a large volume of the most dense matter. This event class should offer the best chance to observe new physics associated with dense matter, e.g., a baryon-rich QGP. However the results summarized below are consistent with no new phenomena being observed.

A baseline comparison for these event-classes has been established by measuring particle spectra over a broad range of centrality. The event classes in this broad range are solely selected on E_{ZCAL}. Both pion and kaon yields increase nonlinearly with the number of participants, and the K^+/π^+ ratio increases with centrality and begins to plateau for the most central reactions. For midperipheral reactions the pion yield per participant increases less with centrality than the kaon yield. The pion yield per participant increases more strongly for central reactions compared to midperipheral reactions.

In the event classes that are doubly selected on event multiplicity and E_{ZCAL}, the yields of π^+ and K^+ trivially increase with multiplicity since the yields in the spectrometer must track the event multiplicity. The K^+/π^+ ratio is examined for any change in behavior that might indicate the onset of new phenomena. However, it is found to be independent of multiplicity for a fixed range of E_{ZCAL}.

From the transverse spectra of particles, the $\langle m_t \rangle - m_0$ for protons is larger than for pions, consistent with transverse expansion. There is no significant change in the proton and pion $\langle m_t \rangle$ in events doubly-selected on E_{ZCAL} and event multiplicity. These events have different proton rapidity distributions implying different conditions in the reaction zone. However there is no observed change in the transverse spectra, even for the high-multiplicity, low-E_{ZCAL} event class that most likely has a large volume of high density matter.

ACKNOWLEDGMENTS

This work was supported by the U.S. Department of Energy under contracts with BNL (DE-AC02-98CH10886), Columbia University (DE-FG02-86-ER40281), LLNL (W-7045-ENG-48), MIT (DE-AC02-76ER03069), UC Riverside (DE-FG03-86ER40271), by NASA (NGR-05-003-513) under contract with University of California, by Ministry of Education and KOSEF (951-0202-032-2) in Korea, and by the Ministry of Education, Science, Sports, and Culture of Japan.

[1] R.J. Glauber, in *Lectures of Theoretical Physics*, edited by W.E. Brittin and L.G. Dungam (Interscience, New York 1959), Vol. 1, p. 315.
[2] E802 Collaboration, T. Abbot *et al.*, Phys. Rev. C **44**, 1611 (1991).
[3] E814/E877 Collaboration, J. Barrette *et al.*, Phys. Rev. Lett. **70**, 2996 (1993).
[4] L. van Hove, Phys. Lett. **118B**, 138 (1982).
[5] M.I. Gorenstein *et al.*, Phys. Lett. B **281**, (1992).
[6] J.I. Kapusta and A.P. Vischer, Phys. Rev. C **52**, 2725 (1995).
[7] E802 Collaboration, L. Ahle *et al.*, Phys. Rev. C **57**, 466 (1998).
[8] T. Abbott *et al.*, Nucl. Instrum. Methods Phys. Res. A **290**, 41 (1990).
[9] L. Ahle *et al.*, Phys. Rev. C **58**, 3523 (1998).
[10] D. Beavis *et al.*, Nucl. Instrum. Methods Phys. Res. A **281**, 367 (1989).
[11] GEANT 3.2.1, CERN Program Library W5013 (1993).
[12] H. Sorge, H. Stöcker and W. Greiner, Ann. Phys. (N.Y.) **192**, 266 (1989).
[13] V. Blobel *et al.*, Nucl. Phys. **B69**, 454 (1974).
[14] H. Fesefeldt *et al.*, Nucl. Phys. **B147**, 317 (1979).
[15] E802 Collaboration, T. Abbott *et al.* Phys. Rev. C **50**, 1024 (1994).
[16] NA44 Collaboration, I.G. Bearden *et al.*, Phys. Rev. Lett. **78**, 2080 (1997).